Electronic structures of amorphous $M_{100-x}Zr_x$ alloys (M = Fe, Co, Ni, Cu) studied using core-level x-ray photoemission spectroscopy

2000 J. Phys.: Condens. Matter 12 5991

(http://iopscience.iop.org/0953-8984/12/27/317)

J. Phys.: Condens. Matter **12** (2000) 5991–6008. Printed in the UK PII: S0953-8984(00)12031-4

Electronic structures of amorphous $M_{100-x}Zr_x$ alloys (M = Fe, Co, Ni, Cu) studied using core-level x-ray photoemission spectroscopy

J-S Kang†, S J Kwon‡, S K Kwon§, K B Lee§ and B I Min§

† Department of Physics, The Catholic University of Korea, Puchon 422-743, Korea
‡ Department of Materials Science and Engineering, Pohang University of Science and Technology, Pohang 790-784, Korea
§ Department of Physics, Pohang University of Science and Technology, Pohang 790-784, Korea

Received 22 February 2000

Abstract. The electronic structures of amorphous a-$Fe_{100-x}Zr_x$ and a-$(Fe_{1-y}M_y)_{33}Zr_{67}$ alloys (M = Co, Ni, Cu) have been investigated by using x-ray photoemission spectroscopy. For a-$Fe_{100-x}Zr_x$, the linewidths of both the Fe 2p and Zr 3d core-level spectra become narrower with increasing x. Systematic line-shape analysis reveals that such a trend could be either due to the decrease in the Auger recombination process or due to the decrease in the exchange splitting of core-hole electrons. The broad Zr 3d spectrum for $x = 10$ is decomposed into two peaks, suggesting a localized nature of the Zr 4d electrons in a-$Fe_{90}Zr_{10}$. For a-$(Fe_{1-y}M_y)_{33}Zr_{67}$ (M = Co, Ni), the Fe 2p spectrum becomes narrower and the shoulder-like satellite structure becomes more pronounced with increasing y, reflecting the increasingly localized nature of the Fe 3d electrons. In contrast, the M 2p spectra of a-$(Fe_{1-y}M_y)_{33}Zr_{67}$ remain essentially unchanged with varying y, implying that the M 2p spectra of a-$M_{100-x}Zr_x$ are much less sensitive to the M ion species than to the fractional concentrations of M and Zr ions. As M varies from Fe to Co and Ni in a-$M_{33}Zr_{67}$, the Zr 3d spectrum exhibits a small shift toward higher binding energy and a slight increase in the linewidth. Band-structure calculations for ordered MZr_2 (M = Fe, Co, Ni, Cu) predict that both the density of states at the Fermi level $N(E_F)$ and the total number of valence electrons increase as M varies from Fe to Co and Ni, which is consistent with the measured Zr 3d spectra of a-$M_{33}Zr_{67}$.

1. Introduction

Amorphous a-$M_{100-x}Zr_x$ alloys (M = Fe, Co, Ni, Cu) exhibit competing effects of spin fluctuations and superconductivity. It is found that the influence of the spin fluctuations on the superconductivity increases as the Zr concentration decreases, except for M = Cu, and also as M moves from Cu toward Fe at a fixed Zr concentration [1]. Recent Mössbauer spectroscopy measurements on a-$(Fe_{1-y}M_y)_{33}Zr_{67}$ alloys (M = Co, Ni, Cu) indicate diverse magnetic ground states [2]. Amorphous a-$Fe_{100-x}Zr_x$ alloys exhibit superconductivity in the low-Fe-concentration range [3], while they exhibit magnetic ordering and Invar-like low thermal expansion in the high-Fe-concentration range [4]. a-$Fe_{100-x}Zr_x$ alloys also possess the ability to absorb hydrogen, but the influence of hydrogenation on the magnetic properties has not been well understood yet. To understand the origin of the diverse magnetic properties in these a-$M_{100-x}Zr_x$ alloys, it is important to investigate their electronic structures systematically.

Photoemission spectroscopy (PES) is one of the experimental methods that determine directly the electronic structures of the solids. There have been several experimental investigations on a-$M_{100-x}Zr_x$ alloys and related materials using valence-band PES and core-level x-ray photoemission spectroscopy (XPS) [5–11]. Band-structure calculations for the

0953-8984/00/275991+18$30.00

related ordered compounds have been carried out to obtain the partial density of states (PDOS) and the core-level shift [6, 12]. Some of the works referred to above have tried to correlate the valence-band PE spectra and the core-level XPS line-shapes with the density of states (DOS) at the Fermi level E_F, $N(E_F)$, and with their magnetic properties [5, 6, 8, 10]. For a-$M_{100-x}Zr_x$, it was concluded that both the M 3d and Zr 4d electrons contribute to $N(E_F)$, and that the fractional contribution of the M 3d electrons to $N(E_F)$ decreases as M changes from Fe to Co, Ni, and Cu.

In this paper, we have investigated the electronic structures of a-$Fe_{100-x}Zr_x$ alloys ($x = 10, 54, 67$) and a-$(Fe_{1-y}M_y)_{33}Zr_{67}$ alloys (M = Co, Ni, Cu) by performing XPS measurements of the M 2p and Zr 3d core levels. a-$(Fe_{1-y}M_y)_{33}Zr_{67}$ alloys (M = Co, Ni, Cu) are paramagnetic and a-$Fe_{100-x}Zr_x$ alloys are ferromagnetic for $x = 10, 54$ with a Curie temperature T_C of about 200 K [3]. We have analysed the Zr 3d and M 2p core-level spectra using the Doniach–Sunjic (DS) line-shape function [13, 14]. We have also performed band-structure calculations on ordered MZr_2 compounds, and compared them to the experimental results.

2. Experimental and computational details

Amorphous a-$(Fe_{1-y}M_y)_{33}Zr_{67}$ (M = Co, Ni, Cu) and Fe_xZr_{100-x} alloy ribbons ($x = 10, 54, 67$), with cross sections of about 10 μm × 2 mm, were prepared by using the rotating-drum technique [15]. The amorphous nature of the ribbons and the nominal compositions were verified by x-ray diffraction (XRD) and electron-probe microanalysis (EPMA), respectively. Core-level XPS measurements were performed using a Perkin–Elmer PHI 5400 ESCA spectrometer. Mg Kα radiation ($h\nu = 1253.6$ eV) was employed as a photon source and a concentric hemispherical analyser was used for the energy analysis of the emitted photoelectrons. The overall instrumental resolution of the system was determined by measuring the full width at half-maximum (FWHM) of the Ag $3d_{5/2}$ peak. For the spectra reported in this paper, the overall resolution was set at a FWHM of about 1 eV. The Fermi level of the system was calibrated by using the binding energy (BE) of the Ag $3d_{5/2}$ peak as 368.3 eV. Samples were cleaned by sputtering with argon ions at a kinetic energy of 3.5 keV until the carbon and oxygen contaminations became negligible. The cleanliness of the measured surfaces was checked by monitoring the carbon (C) 1s and oxygen (O) 1s signals. The base pressure was about 2×10^{-10} Torr. All the measurements on the samples were at room temperature, which belongs to the paramagnetic phase for both a-$Fe_{100-x}Zr_x$ ($x = 10, 54, 67$) and a-$(Fe_{1-y}M_y)_{33}Zr_{67}$ (M = Co, Ni, Cu) [3, 4, 16, 17]. The x-ray satellites due to the Mg K$\alpha_{3,4}$ radiations have been subtracted. The *surface* compositions after sputtering, estimated using core-level XPS data, were close to the nominal compositions of the *bulk*.

Electronic band structures and PDOSs were calculated for ordered MZr_2 compounds (M = Fe, Co, Ni, Cu), by employing the self-consistent LMTO (linearized muffin-tin-orbital) band method within the local density functional approximation (LDA). The $CuAl_2$-type tetragonal structures (space group: $I4/mcm$) and paramagnetic ground states are assumed for all M, except for M = Cu for which $MoSi_2$-type tetragonal structure (space group: $I4/mmm$) is employed [18].

3. Results and discussion

3.1. a-$Fe_{100-x}Zr_x$ alloys

Figure 1 compares the Zr 3d core-level spectra of a-$Fe_{100-x}Zr_x$ alloys ($x = 10, 54, 67$) and that of Zr metal. The spectra are scaled at the $3d_{5/2}$ peak. Our 3d spectrum of Zr metal

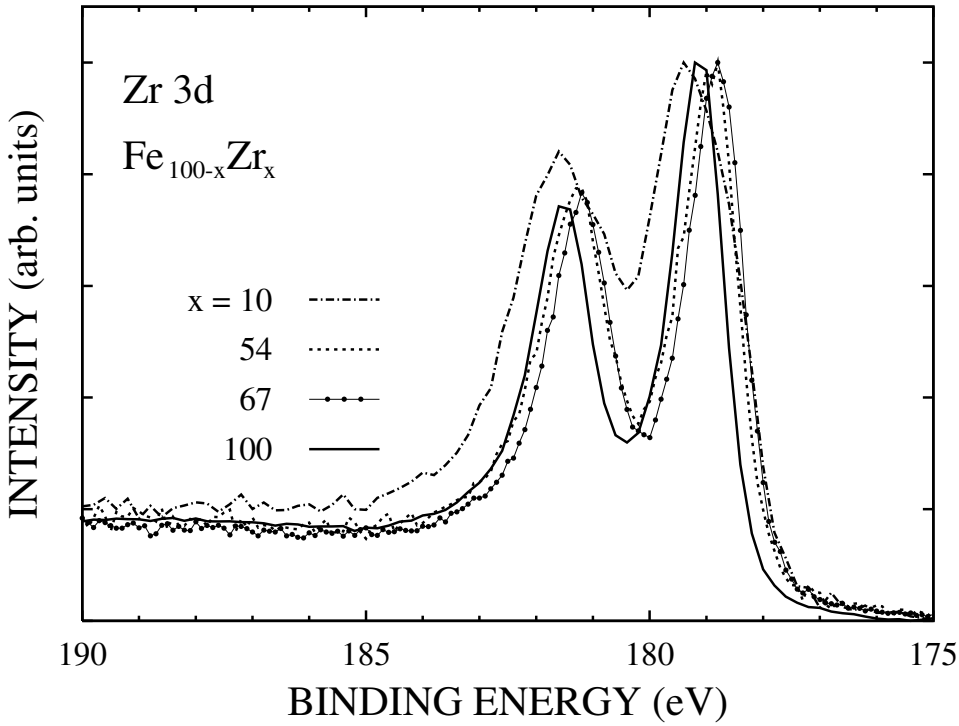

Figure 1. Comparison of the Zr 3d spectra of a-$Fe_{100-x}Zr_x$ ($x = 10, 54, 67$) to that of Zr metal.

represents clean Zr metal [19]. All three spectra show the spin–orbit-split $3d_{5/2}$ and $3d_{3/2}$ components, separated by about 2.4 eV. This figure exhibits the following features. First, the Zr 3d levels in a-$Fe_{100-x}Zr_x$ ($x = 54, 67$) appear at BEs lower by ∼0.3 eV than for Zr metal, reflecting a charge transfer at the Zr ions in a-$Fe_{100-x}Zr_x$ due to the redistribution of the valence electrons [20]. Second, the Zr 3d peaks become broader with decreasing x. In particular, the Zr 3d peaks for $x = 10$ are much broader than those for Zr metal. It will be shown later that this broad feature arises from the two sets of the Zr 3d peaks, one at low BEs and the other at high BEs.

Figure 2 compares the Fe 2p spectra of a-$Fe_{100-x}Zr_x$ ($x = 10, 54, 67$) and Fe metal. The Fe 2p spectra show the spin–orbit-split $2p_{3/2}$ and $2p_{1/2}$ components, separated by about 13 eV. All the spectra are scaled at the Fe $2p_{3/2}$ peak maximum. As x increases, the Fe 2p peaks become narrower. This trend shares a common feature with the Zr 3d spectra. Combining the results of figures 1 and 2, it is found that, as the Zr concentration decreases in a-$Fe_{100-x}Zr_x$, both the Fe 2p and Zr 3d spectra become broader, implying decreasing lifetimes of core holes. Indeed this conjecture is corroborated in tables 1 and 2 below. There are no appreciable core-level BE shifts in the Fe 2p core levels within the instrumental resolution, indicating that the effect of the charge transfer at the Fe ions in a-$Fe_{100-x}Zr_x$ is negligible. All the Fe 2p spectra exhibit rather asymmetric line-shapes. This is probably due to the creation of the electron–hole pairs near E_F subsequent to the emission of the core electron [13,14]. As a first approximation, the asymmetry can be described by a single parameter α. In the case of free electrons, it can be shown that α is proportional to the square of the DOS at E_F, $N(E_F)$ [21]. Further, if the local DOS is approximately constant within a certain energy range around E_F, α is again proportional to the square of $N(E_F)$ [14]. On the other hand, the asymmetric line-shapes also

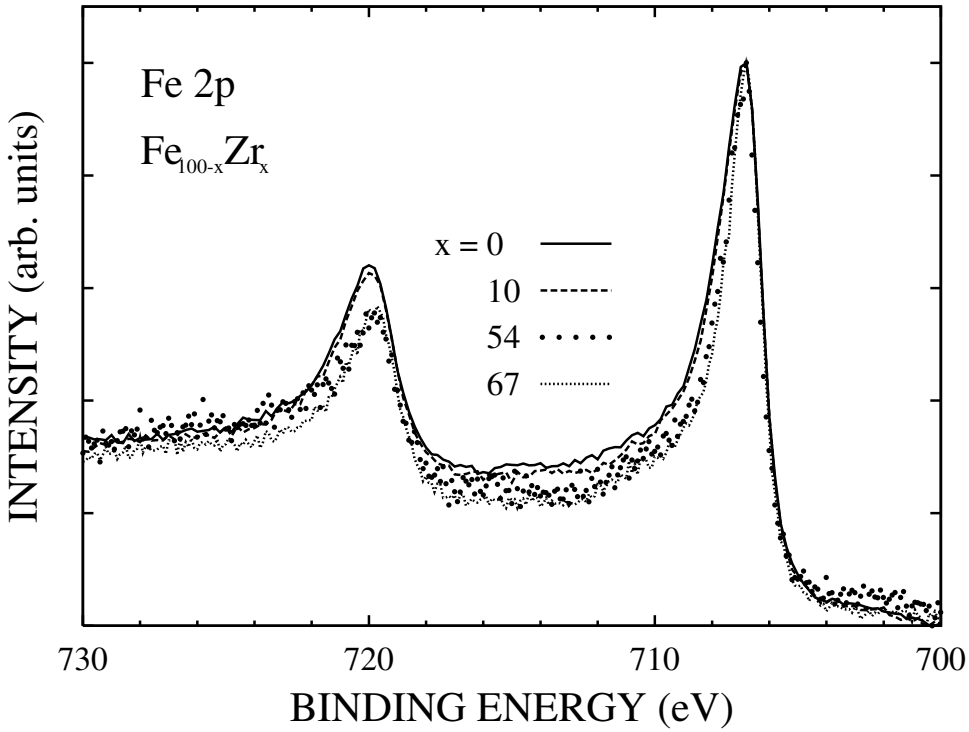

Figure 2. Comparison of the Fe 2p core-level spectra of a-$Fe_{100-x}Zr_x$ ($x = 10, 54, 67$) to that of Fe metal.

suggest that weak satellites might exist at 4–5 eV below the main peaks, due to the Coulomb interaction among the Fe 3d electrons [22]. This point is still controversial [23, 24], and we will discuss it with relation to figures 7 and 8, later.

We have analysed the line-shapes of the Zr 3d and Fe 2p core-level spectra of a-$Fe_{100-x}Zr_x$ alloys, Zr metal, and Fe metal, employing the DS line-shape [13]. The DS line-shape function is a convolution of $1/E^{1-\alpha}$ with a Lorentzian of half-width at half-maximum γ. When $\alpha = 0$, a Lorentzian function is obtained. The DS line-shape function includes two parameters: (i) the linewidth parameter 2γ and (ii) the asymmetry parameter α. The linewidth parameter 2γ, corresponding to the FWHM of the Lorentzian function, is considered to simulate the broadening due to a finite lifetime. Since the lifetime of a core hole is mainly determined by the Auger recombination of the valence electrons, a larger value of the total number of valence electrons N_v will yield a shorter lifetime and consequently a larger 2γ-value. The parameter α represents the asymmetry of the core lines, accounting for the low-energy electron–hole excitations in metals, accompanied by the creation of a core hole. Each peak is further convoluted with a Gaussian function of 1.03 eV FWHM to account for the instrumental resolution. The background due to the inelastically scattered electrons is also added by assuming that the amount of the background is proportional to the total integrated intensity at higher kinetic energies [25]. The multiplet splitting is not included in the curve fitting. This point will be further discussed later.

Figure 3 shows the results of a curve-fitting procedure for the Zr 3d spectra. To fit the Zr 3d spectra, a value of 2.38 eV is used for the spin–orbit splitting between $3d_{5/2}$ and $3d_{3/2}$ components [26], and a value of 0.667 is used for the intensity ratio of the $3d_{3/2}$ to the $3d_{5/2}$

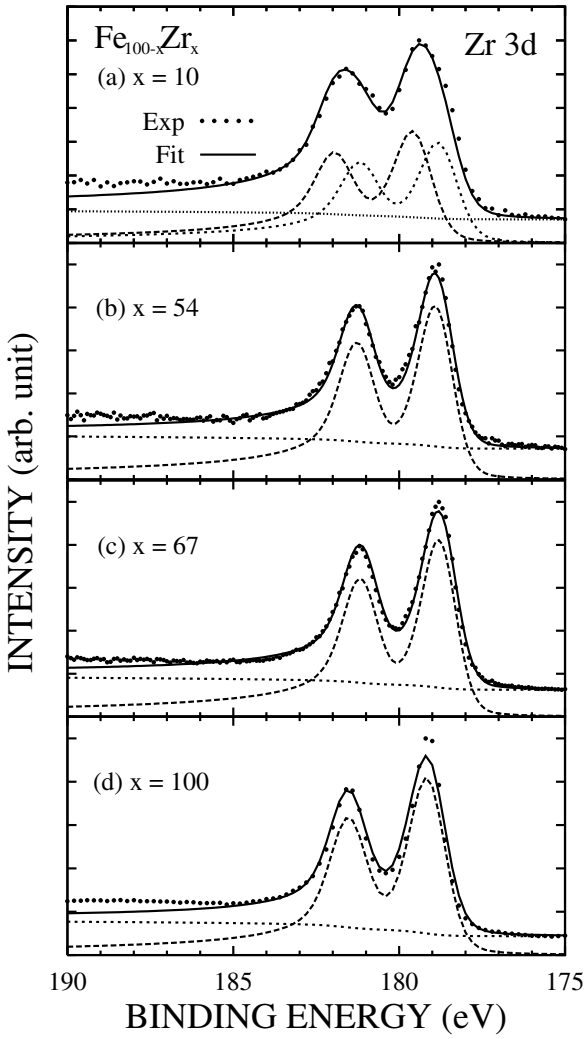

Figure 3. Curve-fitting results (solid lines) for the Zr 3d core levels of a-$Fe_{100-x}Zr_x$ (a) for $x = 10$, (b) for $x = 54$, and (c) for $x = 67$. (d) Similarly for Zr metal. Dots denote experimental XP spectra. Dashed and dotted lines denote the fitting components and the inelastic background, respectively. See the text for the details.

components ($I(3d_{3/2})/I(3d_{5/2}) = 4/6 = 0.667$). Experimental data and the curve-fitting results are denoted as dots and solid lines, respectively. Dashed and dotted lines denote the fitting components and the inelastic background, respectively. In table 1 are listed the

Table 1. Fitting parameters for the Zr 3d spectra of $Fe_{100-x}Zr_x$. 2γ and α represent the FWHM of the Lorentzian function and the asymmetry of the core lines, respectively. ΔE denotes the chemical shift of the $3d_{5/2}$ component in $Fe_{100-x}Zr_x$ with respect to that in Zr metal.

x	BE (eV)	2γ (eV)	α	ΔE (eV)
10	179.44	0.18	0.14	
	178.67	0.17	0.13	−0.37
54	178.80	0.18	0.16	−0.24
67	178.70	0.16	0.15	−0.34
Zr metal	179.04	0.11	0.07	0

parameter values, determined by the curve fitting of the Zr 3d spectra. The curve fitting reveals the following trends. First, the linewidth parameter 2γ for a-$Fe_{100-x}Zr_x$ (0.16–0.18) is larger than that for Zr metal (0.11), implying a shorter lifetime for the Zr 3d core hole in a-$Fe_{100-x}Zr_x$. This difference indicates that the total number of valence electrons available for the Auger recombination in a-$Fe_{100-x}Zr_x$ is larger than that for Zr metal. Second, the asymmetry parameter α for a-$Fe_{100-x}Zr_x$ (0.13–0.16) is also larger than that for Zr metal (0.07), implying a larger $N(E_F)$ for a-$Fe_{100-x}Zr_x$ than for Zr metal. This is probably due to the contribution of the Fe 3d PDOS. Thirdly, for a-$Fe_{90}Zr_{10}$, two-peak structures are required to fit each component of the Zr 3d spectra. The possible origin for the composite structures will be discussed later. The trends in the fitting parameters are consistent with the observation for the Zr 3d spectra in figure 1.

Figure 4 and table 2 show the curve-fitting results for the Fe $2p_{3/2}$ components of a-$Fe_{100-x}Zr_x$, without including the exchange splitting. As the Zr concentration x increases, the magnitude of 2γ decreases, implying decreasing of N_v. Therefore the parameters determined from the curve fitting confirm the finding for the experimental data (see figure 2). Similarly, α decreases with increasing x, indicating decreasing of $N(E_F)$. This finding is consistent with valence-band photoemission spectroscopy results for a-$Fe_{100-x}Zr_x$ (see figure 11(a), later). As mentioned previously, the multiplet splitting has not been included in the analysis of the Fe $2p_{3/2}$ spectra, and so this analysis neglects the changes that can occur in the multiplets with varying x. Thus the energy positions in our curve fitting can be considered to correspond to the weighted averages of the multiplets. The exchange splitting has been neglected in the curve fitting because all the data were taken in the paramagnetic regime above T_C and no evidence was found for local moments in the paramagnetic regime [3]. This feature indicates that the magnetism in a-$Fe_{100-x}Zr_x$ for $x = 10, 54$ could be described well by the itinerant Stoner model, which is consistent with the observed Invar-like behaviour [4].

In order to examine whether local moments possibly persisting above T_C affect the line-shape of the Fe 2p spectra, we have analysed the Fe $2p_{3/2}$ components of a-$Fe_{100-x}Zr_x$ ($x = 0, 10, 54$) by including the exchange splitting Δ_{ex} in the 2p core-hole electrons. The results are presented in figure 5 and table 3. The exchange-splitting analysis has not been applied to the $x = 67$ case because a-$Fe_{33}Zr_{67}$ is paramagnetic in the ground state [3]. For a given x, the lifetime broadening for the majority-spin core hole ($2\gamma_\uparrow$) has been chosen to be larger than that for the minority-spin core hole ($2\gamma_\downarrow$). For simplicity, the asymmetry index α has been chosen the same for both the majority- and minority-spin core-hole states for each x.

It is found that the exchange splitting decreases with increasing x, suggesting that the narrowing of the width with x for a-$Fe_{100-x}Zr_x$ could be due to the decrease in the exchange splitting. This interpretation is valid only when there exist Fe local moments in a-$Fe_{100-x}Zr_x$ even in the paramagnetic regime. On the other hand, table 3 reveals that $2\gamma_\downarrow$ and α also decrease with increasing x, which is consistent with the finding of the previous analysis done without including the exchange splitting. However, in the analysis including the exchange splitting, it was difficult to fit the experimental spectra if the intensity ratio between the minority and majority spins was kept about the same ($I_\uparrow/I_\downarrow \sim 1$) for all x. Further, the quality of the fits is worse when the exchange splitting is included (see figure 5) than when it is neglected (figure 4). To summarize, our analysis does not exclude the possibility that the decrease in the exchange splitting is the origin of the decrease in the Fe 2p linewidth for a-$Fe_{100-x}Zr_x$, which is still consistent with the decrease in N_v and $N(E_F)$. But our analysis indicates that the inclusion of the exchange splitting is not essential in analysing the Fe 2p spectra of a-$Fe_{100-x}Zr_x$ in the paramagnetic regime.

It is interesting that two sets of the Zr 3d peaks are required to fit the data for a-$Fe_{90}Zr_{10}$. Such composite structures may reflect (i) the existence of Zr atoms with different local

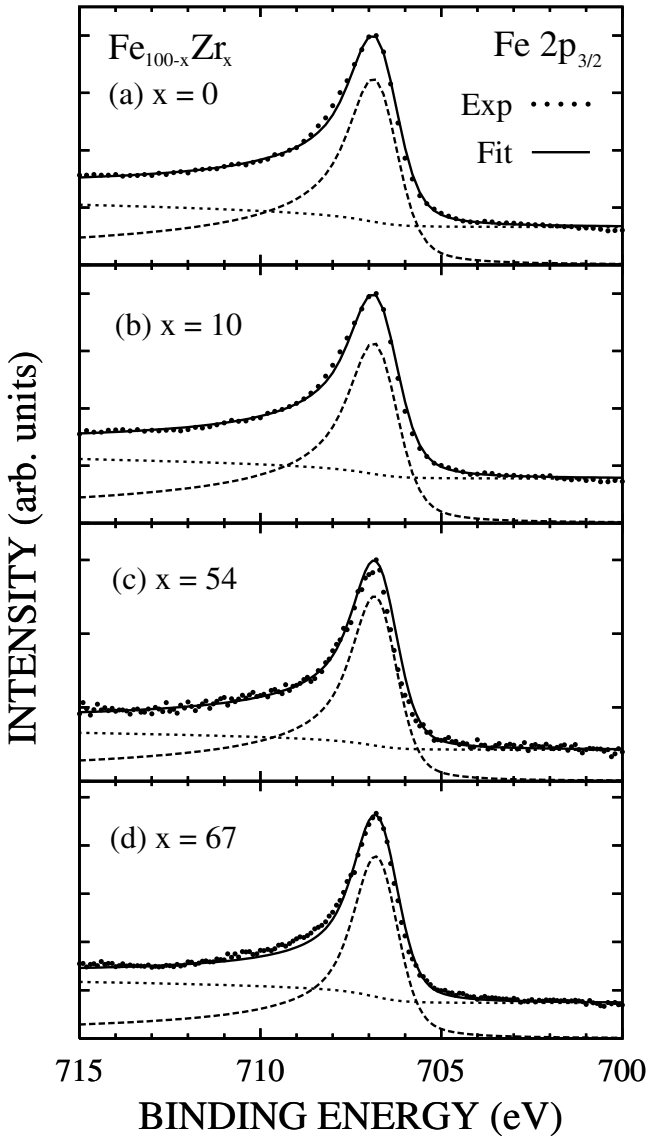

Figure 4. (a) Curve-fitting results for the Fe $2p_{3/2}$ core level of Fe metal without including the exchange splitting. (b)–(d) Similarly for a-$Fe_{100-x}Zr_x$ with $x = 10, 54, 67$, respectively.

Table 2. Fitting parameters for the Fe $2p_{3/2}$ spectra of $Fe_{100-x}Zr_x$ without including the exchange splitting.

x	BE (eV)	2γ (eV)	α
Fe metal	706.60	0.49	0.33
10	706.60	0.48	0.32
54	706.63	0.41	0.29
67	706.63	0.37	0.27

environments, or (ii) different final states screened by different numbers of Zr 4d electrons. If the system was phase separated on a fine scale (a few hundred ångströms) with different local environments around Zr atoms, the material would appear to be amorphous when investigated

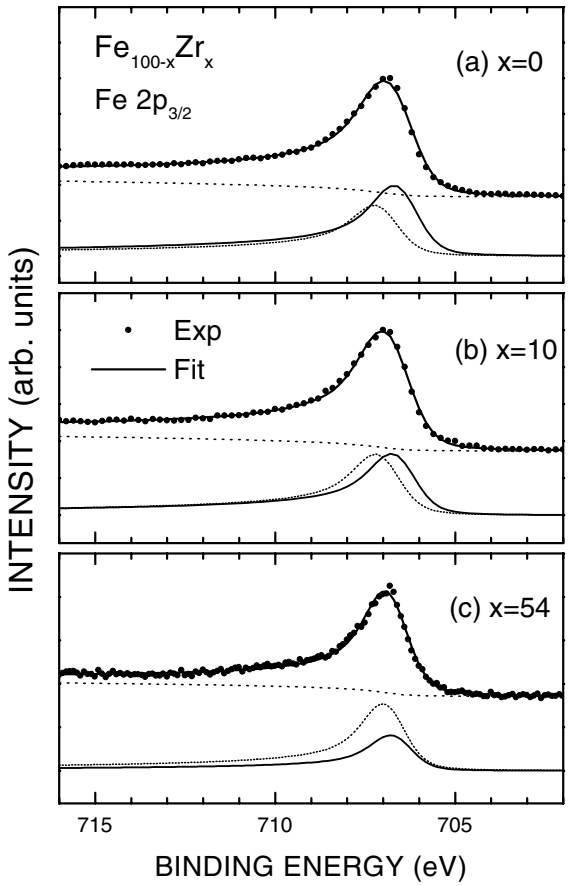

Figure 5. (a) Curve-fitting results for the Fe $2p_{3/2}$ core level of Fe metal including the exchange splitting. (b) Similarly for a-$Fe_{90}Zr_{10}$ and (c) for a-$Fe_{46}Zr_{54}$.

Table 3. Fitting parameters for the Fe $2p_{3/2}$ spectra of $Fe_{100-x}Zr_x$ obtained including the exchange splitting Δ_{ex} between a core hole and the valence electrons. ↑ and ↓ denote the majority-spin and minority-spin core-hole states, respectively.

x	BE(↓)	BE(↑)	$2\gamma_\downarrow$ (eV)	$2\gamma_\uparrow$ (eV)	α	Δ_{ex} (eV)	$I_\downarrow/I_\uparrow$
Fe metal	706.43	706.97	0.36	0.39	0.31	0.54	1.41
10	706.50	706.94	0.35	0.39	0.30	0.44	1.01
54	706.61	706.82	0.33	0.40	0.26	0.21	0.52

by means of x-ray diffraction. Then the Zr core-level spectra would exhibit multiple core-level shifts [27], yielding a continuous broadening in the measured spectra of amorphous alloys.

The second mechanism will also produce several final-state configurations, such as one screened by s, p conduction electrons (a poorly screened final state) and the other screened by the Zr 4d electrons (a relaxed or well screened final state). Assuming the ground-state configuration for a-$Fe_{90}Zr_{10}$ to be $Zr(3d^{10}4d^n)Fe(3d^m)c^l$ (c: Zr and Fe s, p conduction electrons), the poorly screened final-state configurations would be $Zr(3d^9 4d^n)Fe(3d^m)c^{l+1}$ or $Zr(3d^9 4d^n)Fe(3d^{m+1})c^l$ [28]. Similarly, the well screened final-state configurations would be $Zr(3d^9 4d^{n+1})Fe(3d^m)c^l$. This interpretation assumes a localized nature of the Zr 4d electrons

for a-$Fe_{90}Zr_{10}$. Considering the dilute concentration of Zr atoms in these alloys, it is reasonable to assume that Zr 4d electrons are rather localized, as compared to the cases for Zr metal and the Zr-rich regime of a-$Fe_{100-x}Zr_x$.

In the latter interpretation, the low-BE peaks for a-$Fe_{90}Zr_{10}$ are equivalent to the 3d peaks observed for Zr metal ($3d^9 4d^{n'+1} c^{l'}$), with the ground-state configuration of $3d^{10} 4d^{n'} c^{l'}$. This assignment implies that, as compared to those of Zr metal, the Zr 3d core levels of a-$Fe_{100-x}Zr_x$ are shifted to lower BEs, and that the magnitudes of the Zr core-level shifts for a-$Fe_{100-x}Zr_x$ for different x-values are comparable to one another (0.24–0.37 eV) (see table 1). The chemical shift occurs due to the charge redistribution between Zr and Fe ions—that is, the charge transfer from Fe to Zr ions. The direction of the observed Zr 3d core-level shifts toward lower BEs is consistent with the *ab initio* electronic structure calculations shown below (see table 7).

In contrast to the case for Zr 3d spectra, the Fe 2p core levels show no appreciable shifts within the instrumental resolution (see figure 2). This feature suggests that the effect of the charge redistribution on the Fe 2p core levels is negligible in a-$Fe_{100-x}Zr_x$. This can be understood from the fact that the Fe 2p core levels are located very deep in energy, so the effect becomes minor. Indeed, the *ab initio* electronic structure calculations support this argument [29].

3.2. a-$(Fe_{1-y}M_y)_{33}Zr_{67}$ alloys

Figure 6 compares the Zr 3d core-level spectra of a-$M_{33}Zr_{67}$ alloys for M = Fe, Co, Ni, and Cu. The spectra are scaled at the $3d_{5/2}$ peak. Similarly to the case for a-$Fe_{100-x}Zr_x$ (figure 1), all the spectra show the spin–orbit splitting of ∼2.4 eV between the $3d_{5/2}$ and $3d_{3/2}$ components. It is clear that the Zr 3d levels of a-$M_{33}Zr_{67}$ shift to higher BEs as M changes from Fe to Co and Ni, indicating that the charge occupancy at the Zr ions decreases as M varies from Fe to Co and Ni. As will be shown later (table 4), the widths of the Zr 3d peaks increase slightly as M varies from Fe to Co and Ni, implying increasing N_v. These trends in the Zr 3d spectra

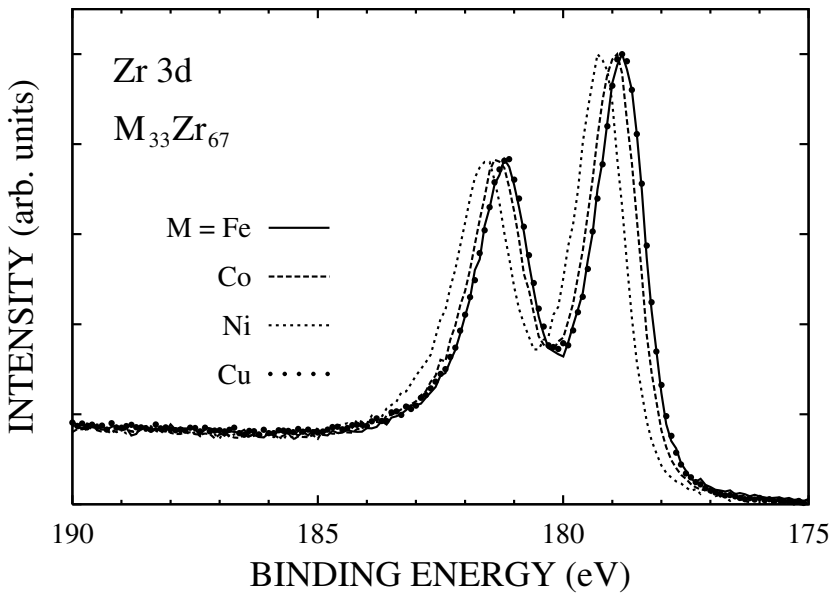

Figure 6. Comparison of the Zr 3d core-level spectra of a-$M_{33}Zr_{67}$ with M = Fe, Co, Ni, Cu.

are consistent with the theoretical calculations for ordered MZr_2 compounds shown in table 7, later. In contrast, the Zr 3d spectrum for M = Cu is almost identical to that for M = Fe.

Figures 7 and 8 compare the M 2p spectra of a-$(Fe_{1-y}M_y)_{33}Zr_{67}$ (M = Co, Ni, Cu; $y = 0.5, 1$) and the Fe 2p spectra of a-$(Fe_{1-y}M_y)_{33}Zr_{67}$ (M = Co, Ni, Cu; $y = 0, 0.5$), respectively. As M varies from Fe to Co, Ni, and Cu, the energy of the spin–orbit-splitting between the $2p_{3/2}$ and $2p_{1/2}$ components increases from about 13 eV to 15 eV, 17 eV, and 20 eV. The Ni 2p spectra clearly exhibit satellite structures at 6–7 eV below the main peaks. The Co 2p spectra also reveal satellites at around 5 eV below the main peaks, weaker than in

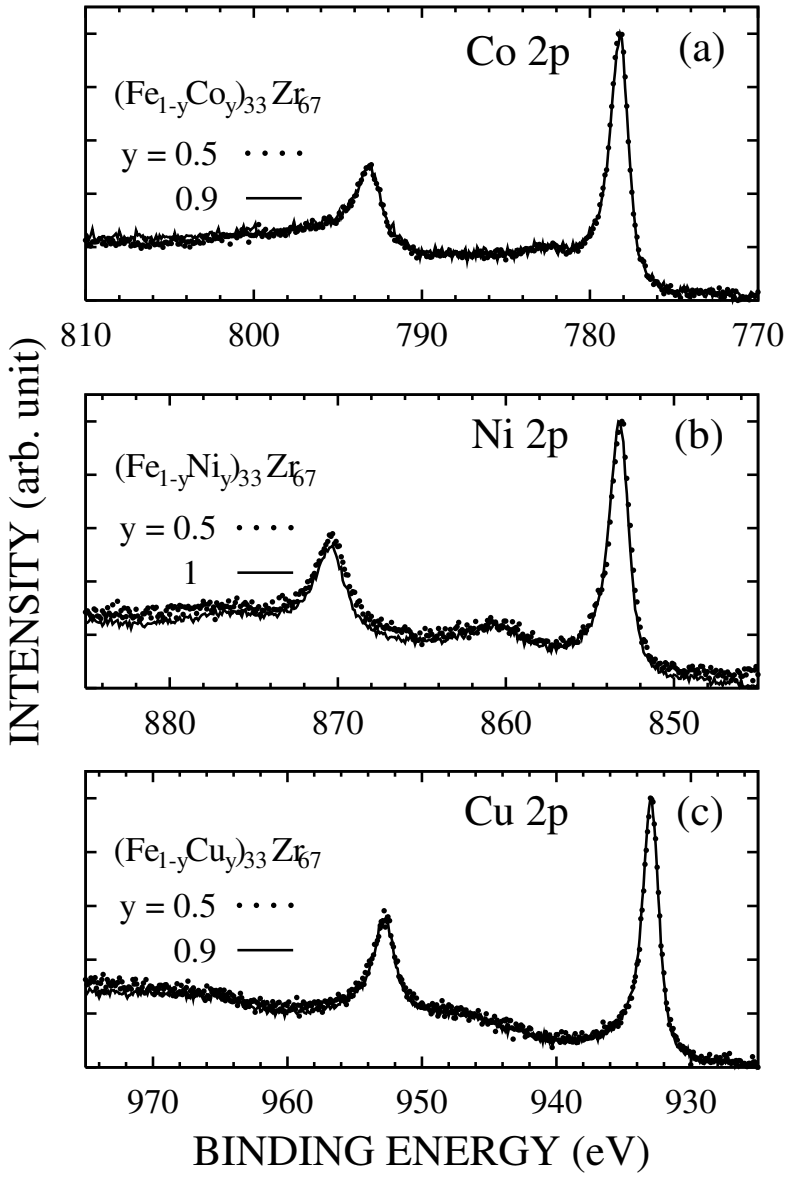

Figure 7. Comparison of the M 2p core-level spectra of a-$(Fe_{1-y}M_y)_{33}Zr_{67}$ with M = Co, Ni, Cu.

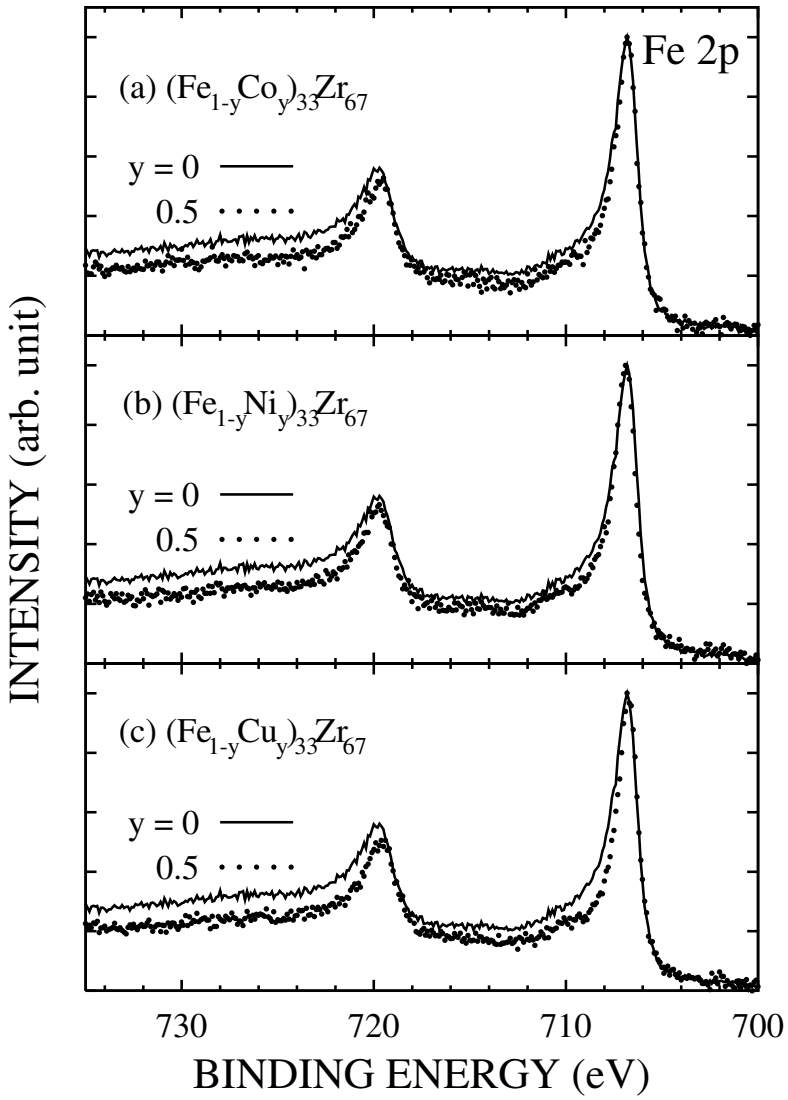

Figure 8. Comparison of the Fe 2p core-level spectra of a-$(Fe_{1-y}M_y)_{33}Zr_{67}$ ($y = 0$ and 0.5) with M = Co, Ni, Cu.

the Ni 2p spectra. It is now realized that the main peaks in the 2p spectra of late transition metals, such as Co and Ni, correspond to the 'well screened' final states, with one more 3d electron than in the initial ground state due to the presence of the strong Coulomb attraction between a core hole and 3d electrons [30]. In this context, the satellite peaks at higher BEs correspond to the 'poorly screened' final states, with the same number of 3d electrons as in the initial ground state [30, 31].

In this framework, the Fe 2p spectra may be similarly interpreted. Very weak shoulder-like structures are observed at about 4 eV below the main peaks in the Fe 2p spectra of figures 2 and 8, which could be assigned to the satellite peaks. As M varies from Ni to Co and Fe, the satellite intensity becomes weaker, and there is a concomitant decrease in the separation

between the satellite and main peaks. Finally, no satellite structures are observed in the Cu 2p spectra. This is due to the filled 3d band, with the initial-state configuration of $3d^{10}c^1$. Note in figure 7 that the M 2p spectra of a-$M_{33}Zr_{67}$ do not change with the Fe substitution for M. This finding reveals that the core-level spectra of a-$M_{100-x}Zr_x$ are much less sensitive to the M ion species than to the fractional concentration of M ions with respect to that of Zr ions (see figure 2, later).

In figure 8, the Fe 2p levels of a-$(Fe_{1-y}M_y)_{33}Zr_{67}$ appear at the same BEs, suggesting no appreciable effect of the charge transfer at the Fe ions with the substitution of Fe for different M elements. With decreasing Fe concentration, the shoulder-like structure at about 4 eV below the main peak becomes more pronounced. As discussed above, the weak shoulder at 4 eV higher BE could be assigned to the satellite. Thus this trend indicates the increasingly localized nature of the Fe 3d electrons with decreasing Fe concentration in a-$(Fe_{1-y}M_y)_{33}Zr_{67}$. The possibility of decreasing values of N_v and $N(E_F)$ with increasing y in a-$(Fe_{1-y}M_y)_{33}Zr_{67}$ is ruled out on the basis of the electronic structure calculations for MZr_2 (see table 7, later).

Figures 9 and 10 and tables 4, 5, 6 show the curve-fitting results for the Zr 3d and M $2p_{3/2}$ spectra of a-$(Fe_{1-y}M_y)_{33}Zr_{67}$. Some discrepancies on the higher-BE sides in figure 10 are due to the neglect of the satellite structures in the curve fitting. Table 4 shows the chemical shifts toward higher BEs from M = Fe to M = Co and Ni, and slightly larger values of 2γ and α for M = Co and Ni than for M = Fe, implying increased N_v and $N(E_F)$ for M = Co and Ni. These fitting results confirm the finding from the experimental data of figure 6. They are also consistent with the valence-band photoemission spectra of a-$M_{100-x}Zr_x$ (M = Fe, Co, Ni; $x = 76$ or 78) in figure 11(b), later.

Table 4. Fitting parameters for the Zr 3d spectra of $M_{33}Zr_{67}$.

M	BE (eV)	2γ (eV)	α	ΔE (eV)
Fe	178.70	0.16	0.15	0
Co	178.87	0.22	0.165	0.17
Ni	179.11	0.225	0.17	0.41
Cu	178.70	0.16	0.15	0

Table 5. Fitting parameters for the M $2p_{3/2}$ spectra of $(Fe_{1-y}M_y)_{33}Zr_{67}$. The fitting parameters are more or less the same for $y \geqslant 0.5$, since the M 2p spectra are essentially the same for $y \geqslant 0.5$ (figure 7).

M	y	BE (eV)	2γ (eV)	α
Fe	1	706.63	0.37	0.27
Co	0.5 0.9	778.10	0.32	0.16
Ni	0.5 1	853.10	0.46	0.11
Cu	0.5 0.9	932.80	0.49	0.11

As to tables 5 and 6, it is non-trivial to determine a unique set of fitting parameters. This is because an exact analysis of the M 2p line-shape is very complicated due to the quantities that influence the line-shapes of the M 2p core-level spectra, such as the Coulomb interaction

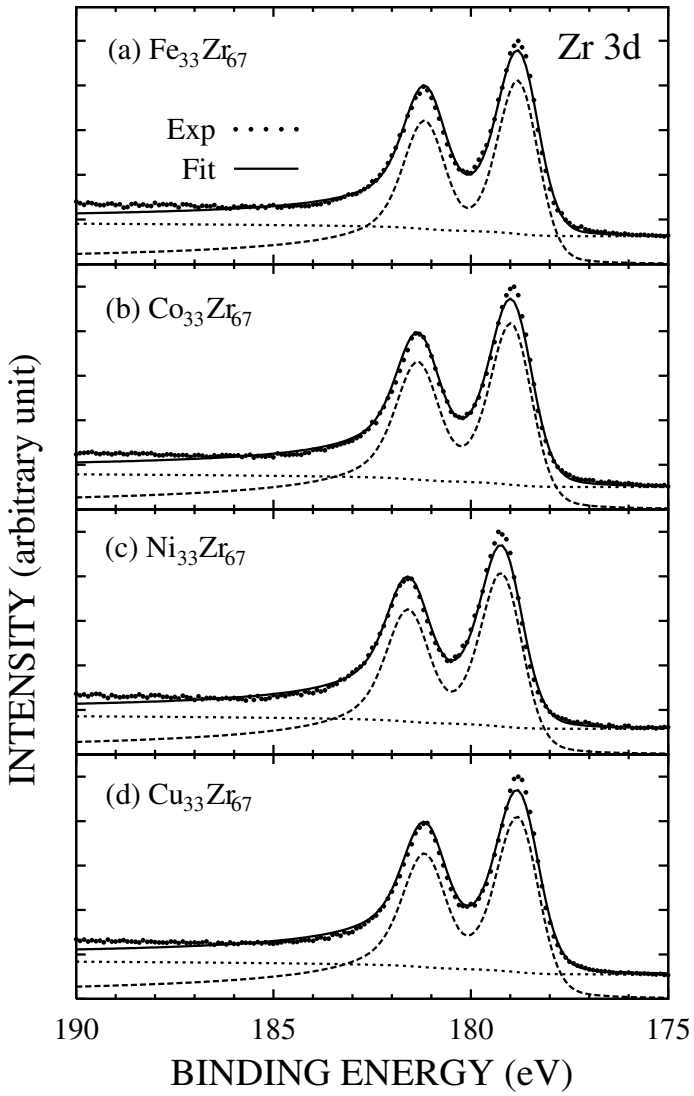

Figure 9. Curve-fitting results (solid lines) for the Zr 3d core levels of a-$M_{33}Zr_{67}$ (a) for M = Fe, (b) for M = Co, (c) for M = Ni, and (d) M = Cu, respectively.

Table 6. Fitting parameters for the Fe $2p_{3/2}$ spectra of $(Fe_{0.5}M_{0.5})_{33}Zr_{67}$.

M	BE (eV)	2γ (eV)	α
$Fe_{33}Zr_{67}$	706.63	0.37	0.27
Co	706.63	0.38	0.18
Ni	706.75	0.36	0.18
Cu	706.61	0.31	0.16

between a core hole and 3d valence electrons, the Coulomb interaction among 3d electrons, the 3d bandwidth and the exchange interaction between a core hole and 3d valence electrons. The core levels of many transition metal oxides and dihalides have been successfully described by

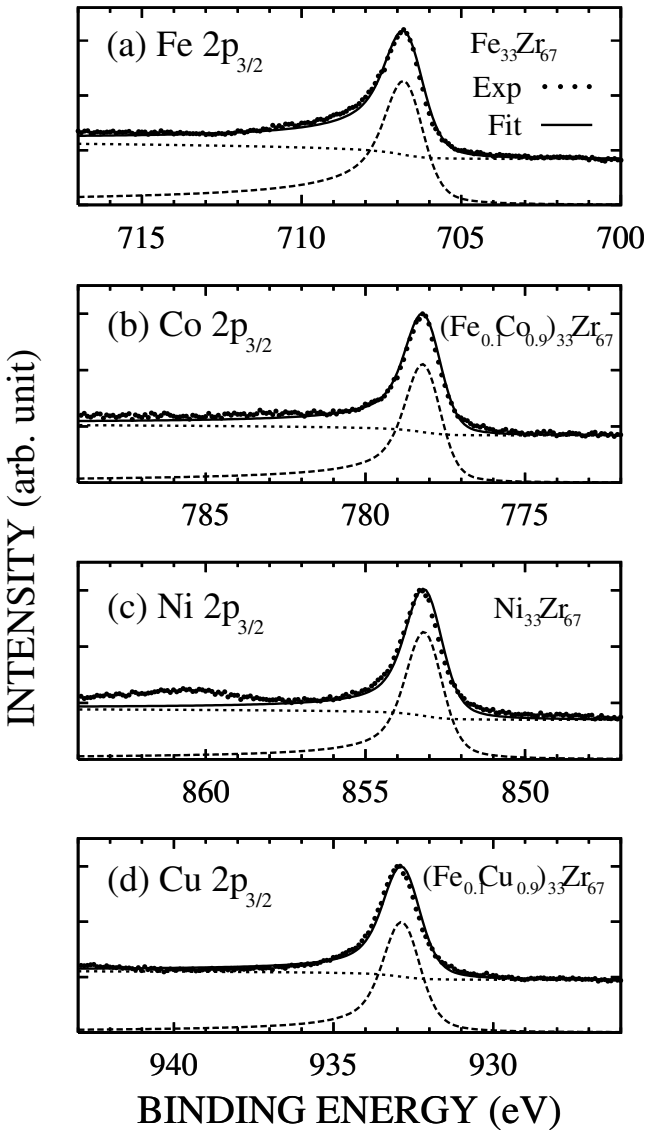

Figure 10. Curve-fitting results (solid lines) for the M 2p core levels of a-$M_{33}Zr_{67}$, compared to the corresponding M 2p XP spectra (dots). (a) M = Fe, (b) M = Co, (c) M = Ni, and (d) M = Cu.

including multiplets in the charge-transfer model [31,32]. Recent studies of thin ferromagnetic Fe films showed that the exchange splitting increases with increasing magnetic moment [33]. Thus it is important to include all these parameters in curve fitting to make an exact analysis of the core-level line-shapes of the transition metal compounds. Note, however, that the core-level line-shapes of itinerant metallic systems in the paramagnetic phase are determined mainly by the lifetime broadening and the asymmetry effect [34]. Therefore both the multiplet and exchange splitting have been neglected in our analysis of M $2p_{3/2}$ spectra of a-$(Fe_{1-y}M_y)_{33}Zr_{67}$. As discussed with relation to figure 5 and table 3, the neglect of the exchange splitting would not be so much of a problem in the interpretation of the analysis, since a-$(Fe_{1-y}M_y)_{33}Zr_{67}$ compounds are paramagnetic in their ground states [3]. As to the neglect of the multiplet splitting, the changes in the local environment of Fe ions with varying y in a-$(Fe_{1-y}M_y)_{33}Zr_{67}$ are expected to be rather small due to their metallic nature. Therefore the fractional changes in

the multiplet splitting and intensities could be neglected, as compared to the energy resolution of our data.

Table 7 shows the calculated values of the PDOS at E_F, $N_l(E_F)$, and the charge occupancy Q_l for ordered MZr_2 compounds (M = Fe, Co, Ni, Cu), obtained from the self-consistent LMTO band calculations. The total number of valence electrons N_v increases steadily in MZr_2 as M varies from Fe to Co and Ni, mainly due to the increasing number of 3d electrons. The total DOS at the Fermi level $N(E_F)$ increases as M varies from Fe to Co and Ni, which is due to the increasing contribution from the Zr PDOS. In contrast, the calculated $N(E_F)$ for M = Cu is substantially lower than $N(E_F)$ for M = Fe, Co, Ni, even though N_v becomes larger. The theoretical calculations for MZr_2 with M = Fe, Co, Ni are consistent with the experimental trends in the Zr 3d spectra of a-$M_{33}Zr_{67}$ (figure 6 and table 4) and the valence-band spectra of a-$M_{100-x}Zr_x$ ($x = 76, 78$) (see figure 11). However, the theoretical results for $CuZr_2$ are inconsistent with the experimental observation that the Zr 3d core-level spectrum of $CuZr_2$ remains nearly unchanged from that of $FeZr_2$. This contradiction remains to be resolved.

Table 7. Calculated PDOSs at the Fermi level $N_l(E_F)$ (states eV^{-1}), total DOSs at the Fermi level $N(E_F)$ (states eV^{-1}/f.u.), charge occupancies Q_l, and the total numbers of valence electrons N_v for ordered MZr_2 compounds. All calculations are performed for paramagnetic states. (f.u. = formula unit).

M		s	p	d	Sum	$N(E_F)$	N_v
Fe	Fe $N_l(E_F)$	0.14	3.18	13.36	16.68		
	Q_l	0.66	0.67	6.58	7.91		
	Zr $N_l(E_F)$	0.31	2.70	7.94	10.95		
	Q_l	0.71	0.77	2.56	4.04	38.58	16.0
Co	Co $N_l(E_F)$	0.10	2.72	8.90	11.72		
	Q_l	0.67	0.68	7.56	8.91		
	Zr $N_l(E_F)$	0.27	2.70	14.05	17.02		
	Q_l	0.70	0.76	2.58	4.04	45.76	17.0
Ni	Ni $N_l(E_F)$	0.27	4.40	7.54	12.21		
	Q_l	0.71	0.69	8.53	9.93		
	Zr $N_l(E_F)$	0.42	5.15	17.77	23.34		
	Q_l	0.69	0.72	2.62	4.03	58.89	18.0
Cu	Cu $N_l(E_F)$	0.11	3.01	1.31	4.43		
	Q_l	0.84	0.62	9.48	10.94		
	Zr $N_l(E_F)$	0.17	2.17	5.80	8.14		
	Q_l	0.69	0.80	2.53	4.02	20.71	19.0

The theoretical predictions could be directly verified experimentally using valence-band photoemission spectroscopy. Earlier valence-band photoemission data seem to support the curve-fitting results for the core-level XP spectra of a-$M_{100-x}Zr_x$ (M = Fe, Co, Ni). This is shown in figure 11, which compares the valence-band photoemission spectra of a-$Fe_{100-x}Zr_x$ ($x = 37, 45, 78$) and those of a-$M_{100-x}Zr_x$ (M = Fe, Co, Ni; $x = 76$ or 78). These data were reproduced from references [10] and [5], where the spectra of a-$Fe_{100-x}Zr_x$ were obtained using He II radiation ($h\nu = 40.8$ eV), and those of a-$M_{100-x}Zr_x$ (M = Fe, Co, Ni) were obtained using He I radiation ($h\nu = 21.2$ eV). In this figure, the spectra of a-$Fe_{100-x}Zr_x$ are normalized to the same height at their maximum peaks, and those of a-$M_{100-x}Zr_x$ ($x = 76$ or 78) are scaled to have the area underneath roughly proportional to 20:21:22 for M = Fe:Co:Ni. The valence-band spectra of a-$Fe_{100-x}Zr_x$ exhibit a gradual decrease in the electronic states

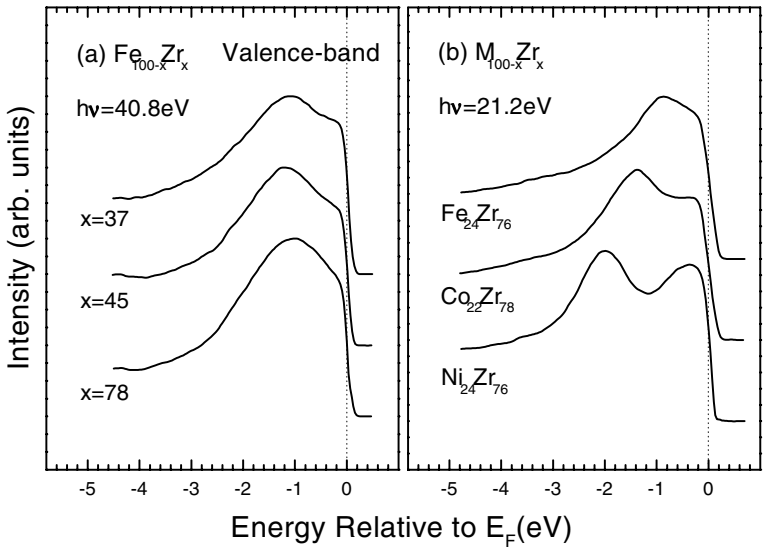

Figure 11. (a) He II ($h\nu = 40.8$ eV) valence-band spectra of a-$Fe_{100-x}Zr_x$ ($x = 37, 45, 78$), reproduced from reference [10]. (b) He I ($h\nu = 21.2$ eV) valence-band spectra of a-$Fe_{24}Zr_{76}$, a-$Co_{22}Zr_{78}$, and a-$Ni_{24}Zr_{76}$, reproduced from reference [5].

at E_F as x increases from $x = 37$ to $x = 78$, implying decreasing $N(E_F)$. For a-$M_{100-x}Zr_x$ ($x = 76$ or 78), the high-BE peaks shift down in energy from M = Fe to M = Co and Ni, with a concomitant build-up of the electronic states near E_F, indicating increasing $N(E_F)$. The high-BE peaks and the peak near E_F for a-$M_{100-x}Zr_x$ can be assigned mainly to the M d states (M = Fe, Co, Ni) and the Zr d states, respectively. The increase in $N(E_F)$ from M = Fe to M = Ni is consistent with the increasing asymmetry parameter α in the Zr 3d spectra of $M_{33}Zr_{67}$ from M = Fe to M = Ni (figure 6 and table 4).

The band-structure calculations for MZr_2 have predicted microscopic differences in the electronic structures of a-$M_{100-x}Zr_x$ for different M elements. The present core-level study of a-$Fe_{100-x}Zr_x$ and a-$(Fe_{1-y}M_y)_{33}Zr_{67}$ (M = Co, Ni, Cu) has also provided valuable information on their valence-band electronic structures. Even though most of the findings in the core-level study agree with the theoretical predictions, some discrepancy has been found between experiment and theory. It is likely that core-level measurements with an improved resolution (using a monochromatized x-ray source or synchrotron radiation) would be appropriate for comparison to theoretical calculations. Further, a more systematic experimental investigation of the valence-band photoemission spectra of a-$M_{100-x}Zr_x$ would provide more detailed information about valence-band electronic structures of these alloys.

4. Conclusions

The electronic structures of a-$Fe_{100-x}Zr_x$ and a-$(Fe_{1-y}M_y)_{33}Zr_{67}$ alloys (M = Co, Ni, Cu) have been investigated by using core-level XPS measurements. For a-$Fe_{100-x}Zr_x$, both the Fe 2p and Zr 3d core-level spectra exhibit decreasing linewidths with increasing x, which could be explained by the decreasing number of valence electrons N_v with increasing x. On the other hand, a detailed analysis which includes the exchange splitting of core-hole electrons shows that the decreasing exchange splitting could also be the origin of the narrower linewidths in the Fe 2p spectra of a-$Fe_{100-x}Zr_x$. However, the fitting quality becomes worse when the

exchange splitting is included, which suggests that the inclusion of the exchange splitting is not necessary for the analysis of Fe 2p spectra of a-$Fe_{100-x}Zr_x$ in the paramagnetic phase. The line-shape analysis of the Zr 3d spectra shows that the Zr 3d spectrum for $x = 10$ consists of two peaks, suggesting the existence of two different final states. This also implies that the Zr 4d electrons in a-$Fe_{90}Zr_{10}$ are rather localized.

In the Fe 2p spectra of a-$(Fe_{1-y}M_y)_{33}Zr_{67}$ (M = Co, Ni, Cu), the peak width becomes narrower with increasing y, accompanied by a more pronounced appearance of the shoulder-like satellite structure. These phenomena indicate that the Fe 3d electrons become more localized as the M concentration increases. With the substitution of Co and Ni for Fe in a-$Fe_{33}Zr_{67}$, the Zr 3d spectra reveal a small shift toward higher BE, with a slight increase in their linewidths. Such trends in the Zr 3d spectra are consistent with the calculated DOS for ordered MZr_2 compounds. The M 2p spectrum of a-$(Fe_{1-y}M_y)_{33}Zr_{67}$ does not change with y, suggesting that the M 2p spectra of a-$M_{100-x}Zr_x$ are much less sensitive to the M ion species than to the fractional concentrations of M and Zr ions. Both the Fe 2p and the Zr 3d core levels are nearly unchanged by Cu substitution. Band-structure calculations for ordered MZr_2 (M = Fe, Co, Ni, Cu) predict that both $N(E_F)$ and N_v increase as M varies from Fe to Co and Ni. For M = Cu, $N(E_F)$ is substantially lower than for M = Fe, Co, Ni.

Acknowledgments

This work was supported by the Korea Science and Engineering Foundation (96-0702-01-01-3 and 1999-2-114-002-5), the Centre for Strongly Correlated Materials Research at SNU, and in part by the Korean MOST-FORT fund. Soon-Ju Kwon thanks Dr Zaven Altounian at McGill University for his help in preparing samples.

References

[1] Altounian Z and Strom-Olsen J O 1983 *Phys. Rev.* B **27** 4149
[2] Dikeakos M, Altounian Z, Ryan D H and Kwon S J 1999 *J. Non-Cryst. Solids* **250–252** 637
[3] Batalla E, Altounian Z and Strom-Olsen J O 1985 *Phys. Rev.* B **31** 577
[4] Shirakawa K, Ohnuma S, Nose M and Masumoto T 1980 *IEEE Trans. Magn.* **16** 910
Ohnuma S, Shirakawa K, Nose M and Masumoto T 1980 *IEEE Trans. Magn.* **16** 1129
[5] Oelhafen P, Hauser E and Güntherodt H-J 1980 *Solid State Commun.* **35** 1017
[6] Moruzzi V L, Oelhafen P, Williams A R, Lapka P, Güntherodt H-J and Kübler J 1983 *Phys. Rev.* B **27** 2049
[7] Fries S M, Wagner H-G, Campbell S J, Gonser U, Blaes N and Steiner P 1985 *J. Phys. F: Met. Phys.* **15** 1179
[8] Neddermeyer H and Paul Th 1987 *Phys. Rev.* B **36** 4148
[9] Bastianon A, Braicovich L and De Michelis B 1992 *Surf. Sci.* **264** 423
Puppin E, Braicovich L, De Michelis B, Vavassori P and Vescovo E 1992 *Surf. Sci.* **264** 429
[10] Cossy-Favre A, Boyen H-G, Oelhafen P, Turek I and Hafner J 1993 *J. Non-Cryst. Solids* **156–158** 246
[11] Kang J-S, Nahm K and Kim C K 1995 *J. Magn. Magn. Mater.* **146** L229
[12] Kübler J, Bennemann K H, Lapka P, Rösel F, Oelhafen P and Güntherodt H-J 1981 *Phys. Rev.* B **23** 5176
[13] Doniach S and Súnjic M 1970 *J. Phys. C: Solid State Phys.* **3** 285
Citrin P H, Wertheim G K and Baer Y 1977 *Phys. Rev.* B **16** 4256
[14] Wertheim G K and Citrin P H 1978 *Photoemission in Solids I* ed M Cardona and L Ley (New York: Springer) p 206
[15] Overhauser A W 1962 *Phys. Rev.* **128** 943
[16] Hiroyoshi H and Fukamichi K 1982 *J. Appl. Phys.* **53** 2226
[17] Ryan D H and Coey J M D 1987 *Phys. Rev.* B **35** 8630
[18] Villars P and Calvert L D 1989 *Pearson's Handbook of Crystallographic Data for Intermetallic Phases* (Materials Park, OH: American Society for Metals)
[19] Wagner C D, Riggs W M, Davis L E, Moulder J F and Mullenberg G E 1978 *Handbook of X-ray Photoelectron Spectroscopy* (Eden Prairie, MN: Perkin-Elmer Corporation)
[20] Sham T K, Perlman M L and Watson R E 1979 *Phys. Rev.* B **19** 539 and references therein

[21] Mahan G D 1990 *Many Particle Physics* (New York: Plenum)
[22] Treglia G, Desjonquères M C, Ducastelle F and Spanjaard D 1981 *J. Phys. C: Solid State Phys.* **14** 4347
Treglia G, Ducastelle F and Spanjaard D 1982 *J. Physique* **43** 341
[23] Chandesris D, Lecante J and Petroff Y 1983 *Phys. Rev.* B **27** 2630
Chandesris D, Lecante J and Petroff Y 1986 *Phys. Rev.* B **34** 8971
[24] Kato H, Ishii T, Masuda S, Harada Y, Miyano T, Komeda T, Onuchi M and Sakisaka Y 1985 *Phys. Rev.* B **32** 1992
Kato H, Ishii T, Masuda S, Harada Y, Miyano T, Komeda T, Onuchi M and Sakisaka Y 1986 *Phys. Rev.* B **34** 8973
[25] There are some other models for the inelastic background. For example, it is found that a power-law background also gives good fits for metallic systems. See Wertheim G K and DiCenzo S B 1985 *J. Electron Spectrosc. Relat. Phenom.* **37** 57
[26] Vaughan D (ed) 1986 *X-ray Data Booklet* (Berkeley, CA: Lawrence Berkeley Laboratory)
[27] Laubschat C, Kaindl G, Schneider W-D, Reihl B and Martensson N 1986 *Phys. Rev.* B **33** 6675
[28] Norman M R, Koelling D D, Freemen A J, Jansen H J F, Min B I, Oguchi T and Ye L 1984 *Phys. Rev. Lett.* **53** 1673
[29] Min B I 1999 unpublished data
[30] Hillebrecht F U, Fuggle J C, Bennett P A, Zolnierek Z and Freiburg Ch 1983 *Phys. Rev.* B **27** 2179
[31] van der Laan G, Westra C and Sawatzky G A 1981 *Phys. Rev.* B **23** 4369
[32] Imada M, Fujimori A and Tokura Y 1998 *Rev. Mod. Phys.* **70** 1039
[33] Huang D J, Riffe D M and Erskine J L 1995 *Phys. Rev.* B **51** 15 170
[34] Hüfner S 1995 *Photoelectron Spectroscopy (Springer Series in Solid-State Sciences vol 82)* (Berlin: Springer) ch 4